Supporting Information

Ratheal et al. 10.1073/pnas.1004214107

SI Methods

Computations. To avoid a straightforward truncation of the large system, which would lead to inaccurate results through the neglect of long-range electrostatic effects, the influence of the surrounding outer region on the atoms of the inner region was incorporated with the general solvent boundary potential in the form of a solvent-shielded static field and a solvent-induced reaction field (1). The reaction field caused by changes in charge distribution of the dynamic inner region is expressed in terms of a basis set expansion of the charge density of the inner simulation region. The basis set coefficients correspond to generalized electrostatic multipoles. Here, a basis set of 400 spherical harmonic functions was used.

Both the solvent-shielded static field and the reaction-field matrix, representing the couplings between the generalized multipoles, were invariant with respect to the configuration of the explicit atoms in the inner simulation region. They were calculated once with the finite-difference Poisson–Boltzmann (PB) model, assuming dielectric constants of 1.0 inside the protein immersed in a solvent with dielectric 78.5. The atomic Born radii for protein and nucleic acid atoms used to set up the dielectric boundaries in the PB calculations were determined by free-energy simulations with explicit solvent (2). The water molecules within the inner region are confined by a nonpolar cavity potential to prevent entry into the surrounding dielectric continuum.

The CHARMM27 force field was used for the protein structure (3). The water molecules were represented by the TIP3P model (4). The reduced system was hydrated with 20 cycles comprising 5,000 steps of Grand Canonical Monte Carlo (5) and 100 ps of Langevin molecular dynamics at 298.15 K with 0.001-fs time steps. A friction constant corresponding to a relaxation time of 5 ps was applied to all the nonhydrogen atoms. The bonds involving hydrogens, and the TIP3 water geometry, were kept rigid using SHAKE (6). All explicit electrostatic interactions beyond 12 Å in the inner region were treated on the basis of dipolar and quadrupolar expansions using the Extended Electrostatic method (EXTE ELEC) (7). This treatment of the nonbonded interactions reduces the computational time by about a factor of 2 relative to a no-cutoff scheme for the entire inner region and avoids the artifacts caused by a truncation of electrostatic interactions. The two acetamidine molecules were docked into the two potassium-binding sites of the X-ray structure by Shinoda et al. (8). The acetamidine molecules were rotated around a randomly picked axis in increments of 30°. The docked complexes were subjected to energy minimization and equilibrated molecular dynamics simulation for 200 ps. One complex structure was simulated further for 20 ns.

1. Im W, Bernèche S, Roux B (2001) Generalized solvent boundary potentials for computer simulations. *J Chem Phys* 114:2924–2937.
2. Nina M, Beglov D, Roux B (1997) Atomic radii for continuum electrostatics calculations based on molecular dynamics free energy simulations. *J Phys Chem B* 101: 5239–5248.
3. MacKerell ADJ, et al. (1998) All-atom empirical potential for molecular modeling and dynamics studies of proteins. *J Phys Chem B* 102:3586–3616.
4. Jorgensen WL, et al. (1983) Comparison of simple potential functions for simulating liquid water. *J Chem Phys* 79:926–935.
5. Woo HJ, Dinner AR, Roux B (2004) Grand canonical Monte Carlo simulations of water in protein environments. *J Chem Phys* 121:6392–6400.
6. Ryckaert J, Ciccotti G, Berendsen H (1977) Numerical integration of the Cartesian equation of motions of a system with constraints: Molecular dynamics of n-alkanes. *J Comput Chem* 23:327–341.
7. Stote RH, States DJ, Karplus M (1991) On the treatment of electostatic interactions in biomolecular simulation. *J Chim Phys* 88:2419–2433.
8. Shinoda T, Ogawa H, Cornelius F, Toyoshima C (2009) Crystal structure of the sodium-potassium pump at 2.4 A resolution. *Nature* 459:446–450.

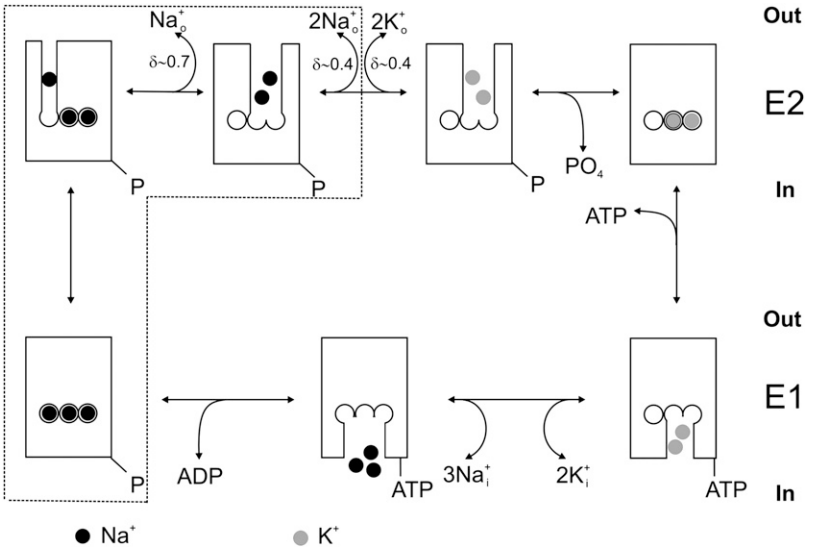

Fig. S1. The Post–Albers scheme overlapped on a cartoon representation of the ion-binding reactions illustrating sequential release of Na^+ ions to the extracellular side. Release of the first ion through a high-field access channel is the most voltage-dependent step in the pump cycle, with the Na^+ ion traversing 70% of the electric field of the membrane (δ = 0.7). Based on mutagenesis studies (1), the Na-exclusive site III appears to be the first one to release.

1. Li C, Capendeguy O, Geering K, Horisberger JD (2005) A third Na+-binding site in the sodium pump. *Proc Natl Acad Sci USA* 102:12706–12711.

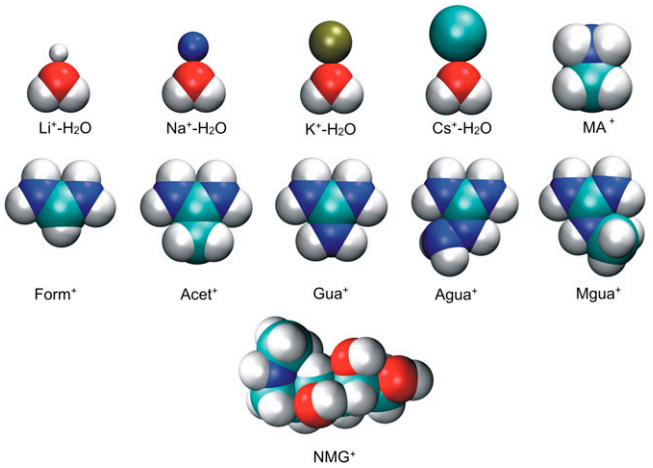

Fig. S2. Space-filling model of the cations studied in this article. Metals are shown with an associated water molecule. $Acet^+$, acetamidinium$^+$; $Agua^+$, aminoguanidinium$^+$; $Form^+$, formamidinium$^+$; Gua^+, guanidinium$^+$; MA^+, methylamine$^+$; $Mgua^+_o$, methylguanidinium$^+$; NMG^+_o, *N*-methyl-D-glucamine^+_o.

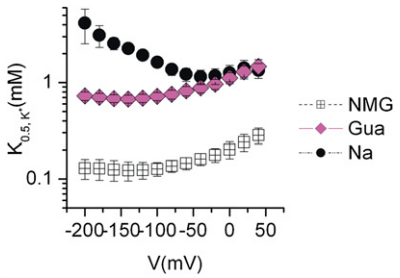

Fig. S3. Gua^+_o reduces K^+_o apparent affinity. Voltage dependence of the half-maximal constant for activation of outward current ($K_{0.5}$) for K^+_o obtained in NMG^+_o, Na^+_o, or Gua^+_o solutions (pH 7.6). The average Hill coefficients were 1.2 ±1 (n = 5) in NMG^+_o, 1.5 ± 0.1 (n = 7) in Na^+_o, and 1.5 ± 0.1 (n = 6) in Gua^+_o.

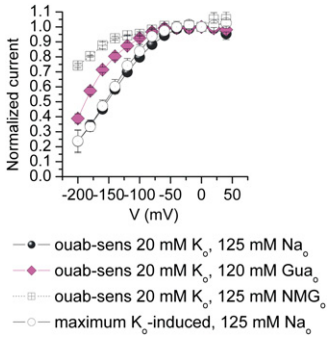

Fig. S4. Voltage dependence of Na/K pump currents at 20 mM K_o^+ in NMG_o^+ (n = 3), Gua_o^+ (n = 7), and Na_o^+ (n = 4) solutions. For comparison, the maximal K^+-induced current calculated from Hill fits in Na_o^+ solutions is shown also (n = 7). Note the close overlap between 20 mM K_o^+ and maximal K_o^+-activated current. Ouab-sens, ouabain-sensitive.

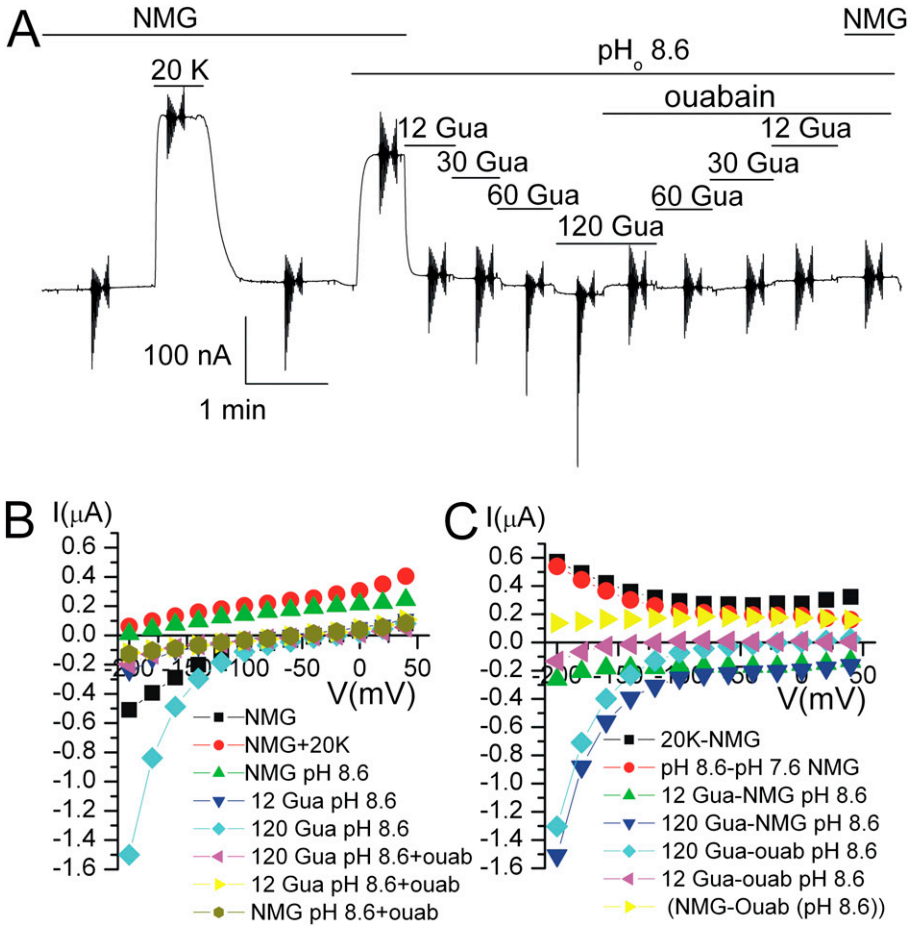

Fig. S5. Effects of Gua^+ at pH 8.6. (*A*) Continuous current recording at a holding potential of −50 mV illustrating the experimental maneuvers performed on a representative oocyte. Application of 20 mM K_o^+ in a 125 mM NMG_o^+ solution at pH 7.6 reversibly induced maximal outward current. Increasing the pH to 8.6 also activated an outward current that was inhibited both by the presence of Gua_o^+, and by ouabain. The brief vertical reflections represent application of 50-ms voltage steps to study the current–voltage relationships in the different solutions. (*B*) Average current during the last 5 ms of the voltage pulses as a function of the applied voltage measured in different conditions (for clarity not all the extracellular conditions in *A* are displayed). (*C*) Subtraction of the different traces in *B* illustrating Gua_o^+ inhibition of the outward current in NMG_o^+ at pH 8.6 together with the current induced by K_o^+ at pH 7.6 and the ouabain-sensitive currents in several ionic conditions at pH 8.6.

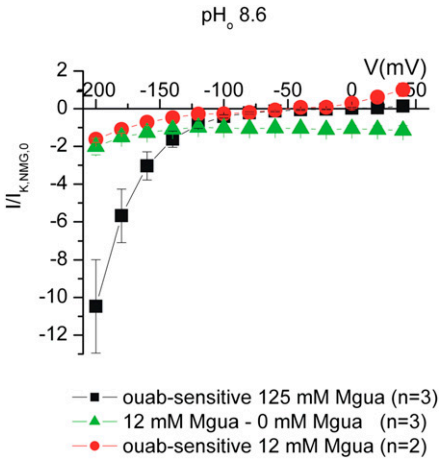

Fig. S6. Effects of $Mgua^+_o$ at pH 8.6. The figure displays the average data from three experiments in which maneuvers similar to those in Fig. S5 were performed with $Mgua^+_o$ solutions instead of Gua^+_o. The I–V curves show the subtracted currents similar to those in Fig. S5C, normalized to the current induced by 20 mM K^+_o in 120 mM NMG^+_o.

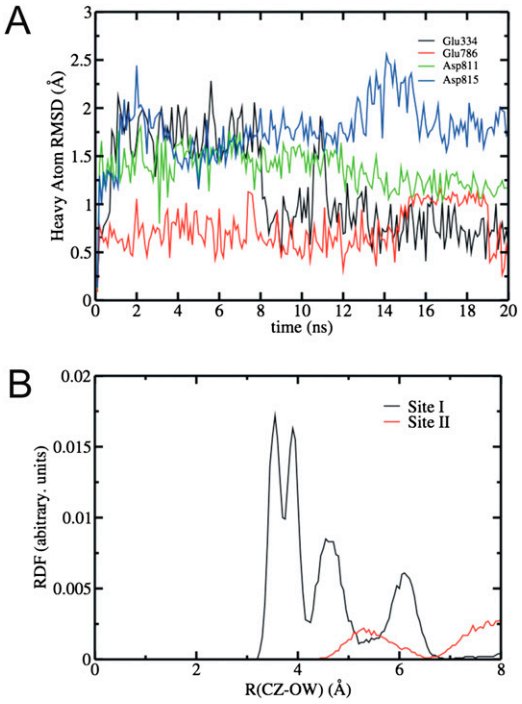

Fig. S7. (*A*) The rmsd of the nonhydrogen atoms in the ion-coordinating acidic residues of the Na/K pump with respect to the starting configuration as a function of the simulation time. (*B*) The radial distribution functions (RDFs) of the water oxygen atom (OW) and the central carbon atom (CZ) of $Acet^+$ in site I and site II.

Table S1. Occurrence of hydrogen bonds between the pump (α)/water (Wat) and the $Acet^+$ ions in site I and site II from the equilibrium simulation

Donor			Acceptor			%
ACET+	NH1	HH11	Wat	HOH	OH2	88.3
ACET+	NH1	HH11	Wat	HOH	OH2	36.1
ACET+	NH1	HH12	α	GLN930	OE1	77.1
ACET+	NH2	HH21	Wat	HOH	OH2	100.0
ACET+	NH2	HH22	α	ASP811	OD1	100.0
ACET+	NH1	HH11	α	ASN783	OD1	96.7
ACET+	NH1	HH12	α	VAL329	O	44.2
ACET+	NH1	HH12	α	ALA330	O	45.2
ACET+	NH2	HH21	α	ASN783	OD1	78.0
ACET+	NH2	HH22	α	ASP811	OD1	100.0
ACET+	NH2	HH22	α	ASP811	OD2	13.6

A geometric criterion was applied to identify the hydrogen bond with the maximum distance of 3.0 Å between the hydrogen atom and the acceptor atom and a minimum donor–hydrogen–acceptor angle of 135°.